Designing Index of Void Structure and Tensile Properties in Wet-Spun Polyacrylonitrile (PAN) Fiber. I. Effect of Dope Polymer or Nonsolvent Concentration

S. Arbab,[1,2] P. Noorpanah,[1] N. Mohammadi,[2] M. Soleimani[2]

[1]*Textile Engineering Department, Amirkabir University of Technology, Tehran, Iran*
[2]*Loghman Fundamental Research Group, Polymer Engineering Department, Amirkabir University of Technology, Tehran, Iran*

Received 30 September 2007; accepted 19 March 2008
DOI 10.1002/app.28458
Published online 30 May 2008 in Wiley InterScience (www.interscience.wiley.com).

ABSTRACT: An index $X\eta^{-1}$ with numerator calculated solely from solubility parameters and denominator measured by on-line viscosity of the fiber precursor in coagulation medium was defined as an indicator of the fiber structure and tensile properties. The $X\eta^{-1}$ values of wet-spun and wound polyacrylonitrile fibers from their dimethylformamide solutions with different polymer concentrations (series A) or nonsolvent concentrations in 10 vol % polymer solutions (series B) into water with draw ratio of one were determined and compared with the corresponding fiber structure and tensile properties. The $X\eta^{-1}$ value of about 0.8×10^6 s^{-1} led to finger-like structure with overall fiber porosity of 82 vol %. By reducing $X\eta^{-1}$ through dope polymer concentration enhancement to 20 vol %, overall fiber porosity decreased to 62 vol % via substitution of some micrometer voids with dense polymer ligament. Accordingly, strong fiber modulus and elongation at break enhancement were observed due to structural defect reduction and cohesive energy density increment. On the other hand, dope nonsolvent concentration increment from 0 to 5 vol % at 10 vol % polymer concentration showed minute overall fiber porosity decrement via $X\eta^{-1}$ increment through micrometer void substitution with nanometer ones (nuclei). Therefore, mild fiber modulus and elongation at break improvements were detected due to defect size reduction which magnifies mechanical properties improvements. Curve fitting of the Wang's second order modulus-porosity correlation to the as-spun fibers modulus-porosity data verified the solid–liquid phase separation through nuclei growth-resistance as the main governing morphological evolution mechanism. © 2008 Wiley Periodicals, Inc. J Appl Polym Sci 109: 3461–3469, 2008

Key words: fibers; nucleation; phase separation; structure-property relations; voids

INTRODUCTION

Guidelines establishment in view of void formation with appropriate size, size distribution and connectivity, and resultant properties of polymeric systems constitutes one of the key issues applicable to diverse technologies such as membrane, foam, and fiber.[1] The porous structure, for example, may facilitate as-spun fiber drawing and on-line dying.[2–7] Phase separation through polymer lean phase nucleation and growth in immersion precipitation process is one of the major practiced approaches toward void formation with controlled morphology. Therefore, elucidation of its effective parameters and their correlation with the resultant void characteristics form one of the most active research fields in polymer science.[8,9] In wet spinning, solvent/nonsolvent exchange rate between fiber precursor and coagulation medium has been mentioned as the main parameter affecting void size, size distribution and morphology.[9–16] Nonsolvent inflow leads to polymer lean phase nucleation often engulfed by polymer rich phase forming core/shell nuclei.[17] Osmotic pressure difference between the polymer lean phase and coagulation medium, then, drives an intrusive mass into the fiber which leads the core of nuclei to grow against polymer rich shells.[11] Therefore, net mixing affinity between fiber precursor and nonsolvent and polymer reach phase rheological resistance determines the exchange rate and demixing time due to phase separation and corresponding void structure. Smolders et al.[18] concluded that instantaneous and delayed demixing often yielded finger-like and sponge-like structures, respectively. Precipitant addition to dope or spinning solution, for example, affects demixing time via reducing the rate of solvent outflow and nonsolvent inflow both rheologically and thermodynamically. In other words, assuming constant exchange rate of solvent outflow and nonsolvent inflow, dope containing less precipitant would show the least viscosity, fastest phase separation, and finger like void formation. Precipitant addition, however, strongly affects pair wise interactions among polymer-nonsolvent, polymer-

Correspondence to: N. Mohammadi (mohamadi@aut.ac.ir).

solvent and solvent-nonsolvent which often lead to mass transfer rate decrement between the dope and nonsolvent. According to the calculations and modeling by Yilamz and Machugh[19] and Tsay and Machugh,[20] an increase in solvent/nonsolvent interaction parameter (χ_{13}) enhances the miscibility gap in the phase diagram which corresponds delayed demixing. Furthermore, their results verify miscibility gap decrement via polymer/solvent (χ_{12}) or polymer/nonsolvent (χ_{23}) interaction parameter increment leading to instantaneous demixing. On the basis of aforementioned qualitative data evaluations, Ruaan et al.[21] proposed ϕ criteria for selecting solvent and coagulation medium in view of macrovoid formation in the wet phase inversion process:

$$\phi = \frac{\Delta\delta_{p-s}\Delta\delta_{p-\mathrm{ns}}}{\delta_p \Delta\delta_{s-\mathrm{ns}}} \quad (1)$$

where $\Delta\delta_{p-s}$, $\Delta\delta_{p-\mathrm{ns}}$, and $\Delta\delta_{s-\mathrm{ns}}$are solubility differences among polymer-solvent, polymer-nonsolvent and solvent-nonsolvent, respectively, while δ_p is polymer solubility parameter. By addition of nonsolvent to dope or solvent to coagulation medium, however, $\Delta\delta_{p-s}$ and $\Delta\delta_{p-\mathrm{ns}}$ are substituted with $\Delta\delta_{p-\mathrm{ms}}$ and$\Delta\delta_{p-\mathrm{mns}}$, respectively, where m stands for mixed solvents or nonsolvents. Using ϕ criterion, Ruaan et al.[21] proceeded to predict correctly void morphologies in some wet phase inversing systems while they also reported some discrepancies. In addition, van de Witte et al.[22] got membranes with void structures on the contrary with what was expected based on phase separation time scale. In other words, nonsolvent addition to the dope in their systems led to shorter delayed time contrary to what was anticipated. On the other hand, the role of polymer reach phase rheological resistance against polymer lean phase (nuclei) growth during morphological evolution in wet phase inversion process was often ignored by many research groups or considered just qualitatively.

The effects of void structure on product final properties have also been studied by many research groups [3, 4, 23, 24, and 25]. Stoyanov[23] reported fiber strength increment due to its density fluctuation decrement through dope polymer concentration enhancement in wet spun PAN fiber. In addition, Beder et al.[24] found porosity decrement and mechanical properties improvement in a wet spun PAN fiber via solvent addition to the coagulation medium. On the other hand, Bahrami et al.[3] demonstrated mechanical properties decay in wet spun acrylic fibers by rising the temperature of coagulation medium. They attributed their observations to micrometer size void formation and reduced fiber orientation and crystallinity. Quite recently, Dutriez et al.[25] concluded void size reduction to nanometer scale as the prerequisite of drastic improvements in mechanical properties of polymers such as crack growth rate decrement and toughening. Trying to correlate the mechanical properties of porous objects to their microstructures, Sonnenschein[26] fitted the modulus-porosity curves of their membranes to the Wang and Eshpriegs' models and concluded their morphological evolution mechanisms. In other words, Wang's second order equation fits the modulus-porosity curves of low porosity systems with mainly nodular structures made via solid-liquid phase separation. Although, Eshpriegs' first order equation suits modulus-porosity relationships of high porosity systems mainly prepared via liquid–liquid phase separation.

In this research work, an index $X\eta^{-1}$ combining aggressive and resistive based parameters of phase separation through immersion precipitation was introduced for estimating fiber structure and tensile properties. Curve fitting of the acquired experimental modulus-porosity data by the aforementioned models was also used for delineating corresponding void evolution mechanisms.

EXPERIMENTAL

Materials

Poly (acrylonitrile-*ran*-methylacrylate) (94/6 wt %) was received from Polyacryl Co. (Isfehan, Iran). Dimethylforamide (DMF) from (BDH chemicals) and tap water were used as solvent and nonsolvent, respectively.

Copolymer characterizations

Viscosity, average molecular weight and molecular weight distribution, PDI, of the copolymer were measured by intrinsic viscosity of dilute solution in 30°C DMF and gel permeation chromatography (GPC 150 C, Waters) in 30°C tetrahydrofurane (THF), respectively. Fourier transform spectroscopy (Nicollet 670) was also used to verify copolymer composition.

Fiber spinning and dope on-line viscosity measurement

Two groups of dope were prepared and used for spinning. In group number one or series A, polymer particles, M_v = 70,000 g/mol and PDI = 3.2, were swelled for 24 h in 40°C DMF and later mixed to homogeneous solutions with 10 up to 20 vol % polymer concentration, Table I. In the second group, series B, 1.5, 3, and 5 mL out of 100 mL solvent in 10 vol % polymer solutions of series A were replaced with distilled water, Table I. The aforementioned solutions were wet spun through a single spinneret

TABLE I
Recipes of Dope Solutions in Vol % Used for Wet Spinning

	A 10	B 1.5	B 3	B 5	A 12	A 16	A 20
DMF	90	88.5	87	85	88	84	80
Water	0	1.5	3	5	0	0	0
PAN	10	10	10	10	12	16	20

with a diameter of 200 μm and $L/D = 1$ using a metering pump (pump constant 0.5 cc/rev.) into one meter long coagulation medium at room temperature and wound on a bobbin with draw ratio of one. On-line dope viscosity evaluation was performed via measuring the spinneret back pressure and flow rate.

Porosimetry

Overall porosity of as-spun and dried (24 h at ambient temperature) fibers was characterized by weight and volume measurements on at least 50 one meter long replicates from randomly selected regions of wound fibers. Fiber diameter was determined by optical microscopy (Carl Ziess 533) while fiber porosity was calculated using following equation:

$$\text{Overall porosity(vol \%)} = \frac{\pi R^2 L - m\rho_p^{-1}}{\pi R^2 L} \times 100 \quad (2)$$

where R, L, and m are fiber radius, length and mass, respectively, while ρ_P is polymer density.

Thermoporometry

Fiber thermoporometry was conducted using differential scanning calorimetry (DSC 2010, TA Instrument) on water saturated samples. Three to six milligrams of water saturated fibers were sealed and freezed to −60°C in aluminum pan and then heated with a rate of 1°C/min. For instrument calibration, Indium (ΔH_f = 0.014 cal/g) was applied, while aluminum pan itself was used as the reference. For each sample, measurement was performed on three replicates and the average results were reported.

Electron microscopy

As-spun and dried fibers were freeze fractured in liquid nitrogen, coated with a thin layer of gold and scanned with an electron microscope (Cambridge ST360).

Tensile measurements

Fibers with gauge length of 2.5 cm were clamped and drawn with a rate of 25 mm/min on tensile machine (Instron 5565) up to rupture and their mechanical characteristics were determined. For each sample at least 15 replicates were characterized and the average values reported.

RESULTS AND DISCUSSION

Figure 1 shows overall porosity of as-spun fibers versus dope polymer concentration, series A (a), and nonsolvent concentration, series B (b), respectively. Dope polymer concentration, or nonsolvent concentration enhancement decreased overall fiber porosity. The porosity decrement, however, is much steeper via dope polymer concentration increment in the studied range. Raising dope polymer concentration or nonsolvent concentration in 10 vol % polymer solution reduced thermodynamic affinity toward mass exchange between fiber precursor and nonsolvent while increased dope solution viscosity. Accordingly, dope polymer concentration increment gradually decreased the number and length of finger-like channels (micrometer voids) extended from surface to center of the fibers, Figure 2. Nonsolvent concentra-

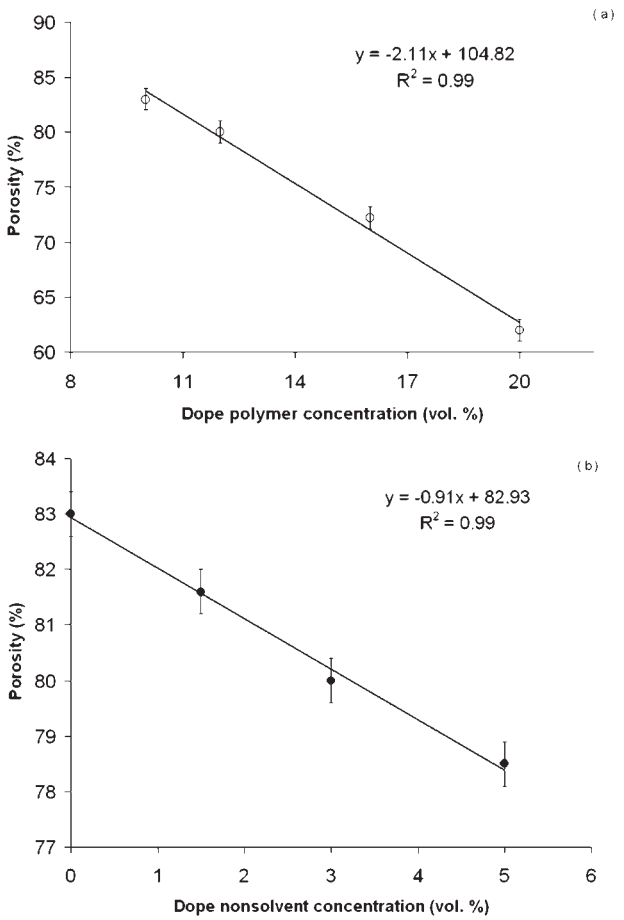

Figure 1 Effect of dope polymer concentration (a) and nonsolvent concentration in 10 vol % polymer solution (b) on fiber overall porosity.

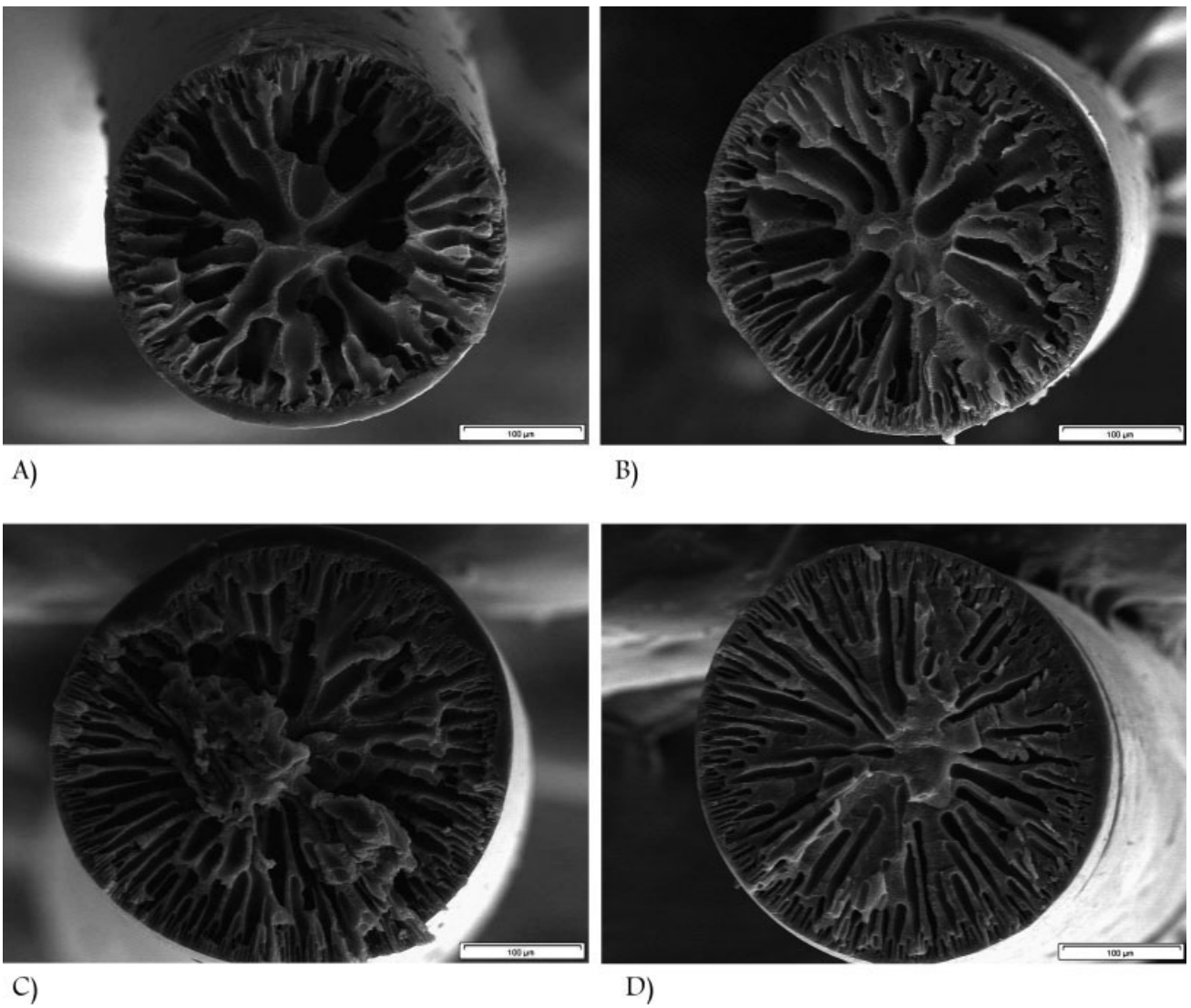

Figure 2 Effect of dope polymer concentration on cross-sectional morphology of as-spun PAN fibers: (A) 10 vol %, (B) 12 vol %, (C) 16 vol %, and (D) 20 vol %.

tion increment in 10 vol % polymer solution, however, eventually increased the number and decreased the width of the finger-like channels, Figure 3. Detail morphological evolution of the wet spun fibers prepared by immersion precipitation process was also studied by thermoporometry, Figure 4. The main advantage of this technique is the possibility of quantifying fiber nanometer voids fraction based on integrating heat flow area due to water fusion with melting temperature below 0°C, Table II. DSC heat flow curves may also be sliced to quantify each nanometer size void fraction according to the well-known theories and equations,[27] Figure 5. On the other hand, image analysis based on a Mat lab computer program was used to quantify the micrometer voids (macro voids) fractions of as-spun fibers, Table II. Therefore, the volume fraction of polymer ligament engulfing fiber micrometer or nanometer size voids was deduced by subtracting total void volume from overall fiber volume, Table II. Rising dope polymer concentration from 10 to 12 vol. % enhanced nanometer voids fraction from 21 to 23 vol %. Further polymer concentration increment to 16 vol %, however, increased nanometer voids to 28 vol %. It worth's mentioning that dope polymer concentration increment simultaneously decreased fiber micrometer voids via its dense ligament increment along with nanometer voids size and size distribution decrement, Table II and Figure 5. Dope polymer concentration enhancement forbids mainly rheologically nanometer voids (nuclei) growth to larger sizes due to nonsolvent intrusion during immersion precipitation. Accordingly, more uniform and smaller nanometer voids are formed with dope polymer concen-

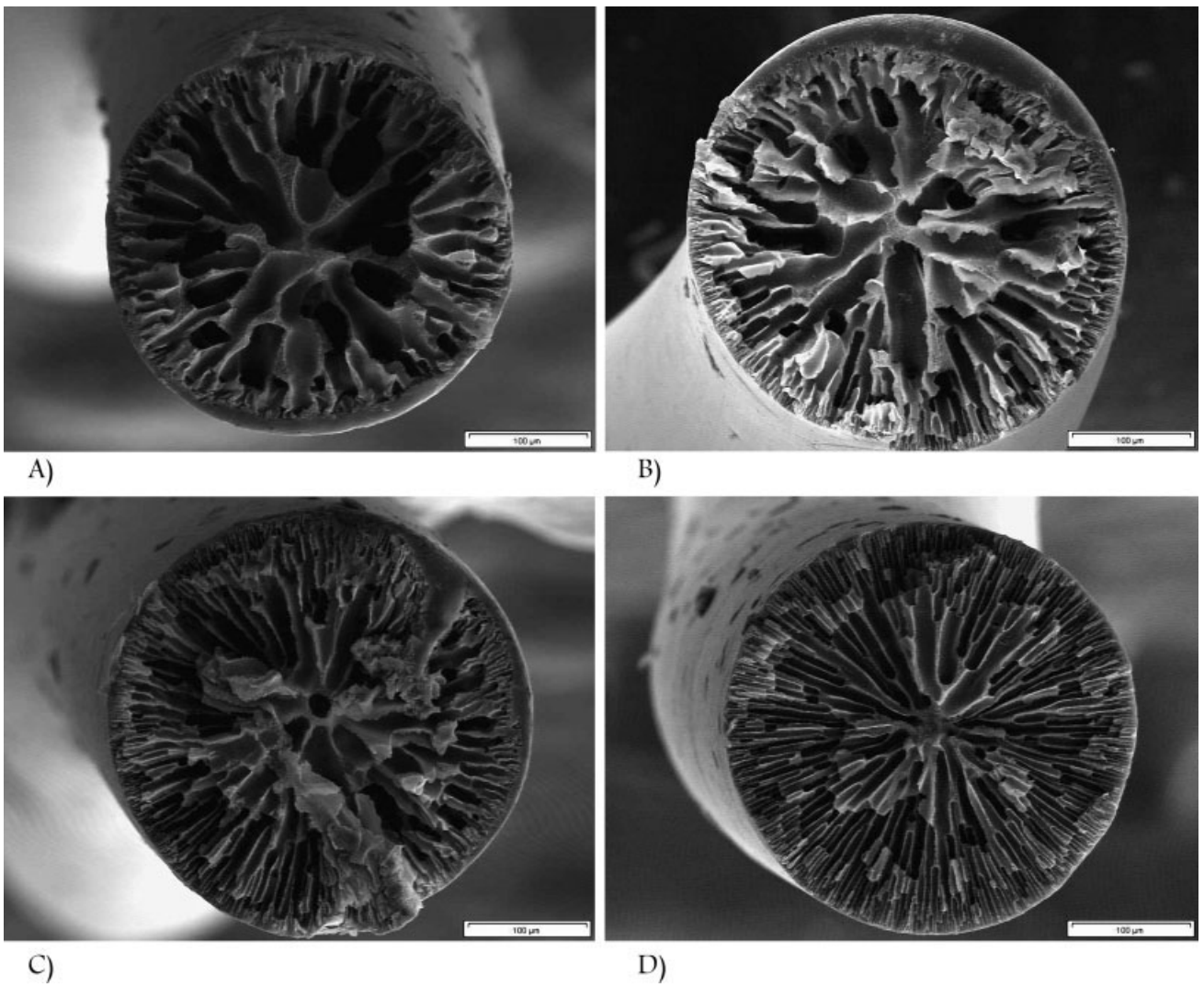

Figure 3 Effect of nonsolvent concentration in 10 vol % polymer solution on cross-sectional morphology of as-spun PAN fibers: (A) 0 vol %, (B) 1.5 vol %, (C) 3 vol %, and (D) 5 vol %.

tration increment, Figure 5. On the other hand, dope nonsolvent increment from 0 to 5 vol % in 10 vol % polymer solution reduced fiber micrometer voids by 16.5 vol % while provided about 15 vol % of nanometer voids and 4.5 vol % dense ligament increments. Therefore, dope nonsolvent increment at constant polymer concentration mainly led to void morphology change in as-spun fibers.

Thermodynamic affinity of fiber precursor to nonsolvent was estimated by using eq. (3) to keep with the spirit of the Machugh[19,20] and Smolders et al.[18]:

$$X = \frac{\Delta\delta_{p-s}^2 \Delta\delta_{p-\mathrm{ns}}^2}{\Delta\delta_{s-\mathrm{ns}}^2} \quad (3)$$

The basis for replacing $\Delta\delta^2$ in place of proposed $\Delta\delta$ in Ruaan et al. ϕ parameter for pair wise interaction evaluation among components is the proportionality

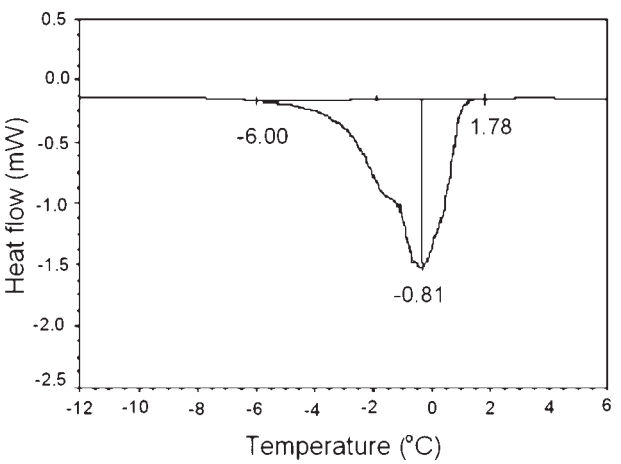

Figure 4 Typical DSC heat flow curve of ice melting in saturated porous as spun fiber.

TABLE II
Volume Fractions of Micrometer Voids, Nanometer Voids and Dense Polymer Ligament Where Constitute As-Spun Fibers of Dope Compositions

Dope identification	Micrometer voids (vol %)	Nanometer voids (vol %)	Dense polymer ligament (vol %)
A10	62.5	21	16.5
B1.5	45.5	36	17.5
B3	45	34.0	20.5
B5	46	32.5	21
A12	57	23	20
A16	45	28	24
A20	40	22	38

of χ_{ij} with $\Delta\delta_{ij}^2$.[21] For considering the rheological barrier against nonsolvent intrusion and nuclei growth,[17] however, an index was defined by dividing X over fiber on-line viscosity:

$$X\eta^{-1} = \frac{\Delta\delta_{p-s}^2 \Delta\delta_{p-\mathrm{ns}}^2}{\eta \Delta\delta_{\mathrm{s-ns}}^2} \quad (4)$$

$\Delta\delta_{ij}^2$ are calculated by adding square of solubility differences between dispersive, polar and hydrogen bonding components of the constituents. The thermodynamic affinity, X, and on-line viscosity, η, terms of fiber precursor toward nonsolvent were plotted versus dope polymer concentration in Figure 6. Although, fiber on-line viscosity increased dramatically with dope polymer concentration, its thermodynamic affinity toward nonsolvent stayed constant. Normally, χ_{12} ($\Delta\delta_{p-s}^2$) varies with composition of polymer solution and its dependence on polymer concentration, ϕ_2, is often estimated quantitatively by relation of the Koningsveld and Kleintjens[28]:

$$\chi = \alpha + \frac{\beta(1-\gamma)}{(1-\gamma\phi_2)^2} \quad (5)$$

Where α,β and γ are constants for a given system and temperature. For polystyrene in cyclohaxane solutionχ_{12} or its enthalpy component was reported almost constant in the concentration range of 0.1–0.2.[29] Therefore, χ_{12} was also considered constant for ϕ_2 variation between 0.1 and 0.2 in the current system.

On the other hand, dope nonsolvent concentration enhancement in 10 vol. % polymer solution decreased fiber affinity toward coagulation medium (X enhancement) and increased its on-line viscosity simultaneously, Figure 7. Dope viscosity increment with polymer concentration enhancement, however, was much stronger compared with its dependence on dope nonsolvent concentration. The effect of nonsolvent addition to the dope was estimated through $\Delta\delta_{\mathrm{p-ms}}^2$ and $\Delta\delta_{\mathrm{ms-ns}}^2$ parameters in place of $\Delta\delta_{\mathrm{p-s}}^2$ and $\Delta\delta_{\mathrm{s-ns}}^2$, respectively. More exact calculations of

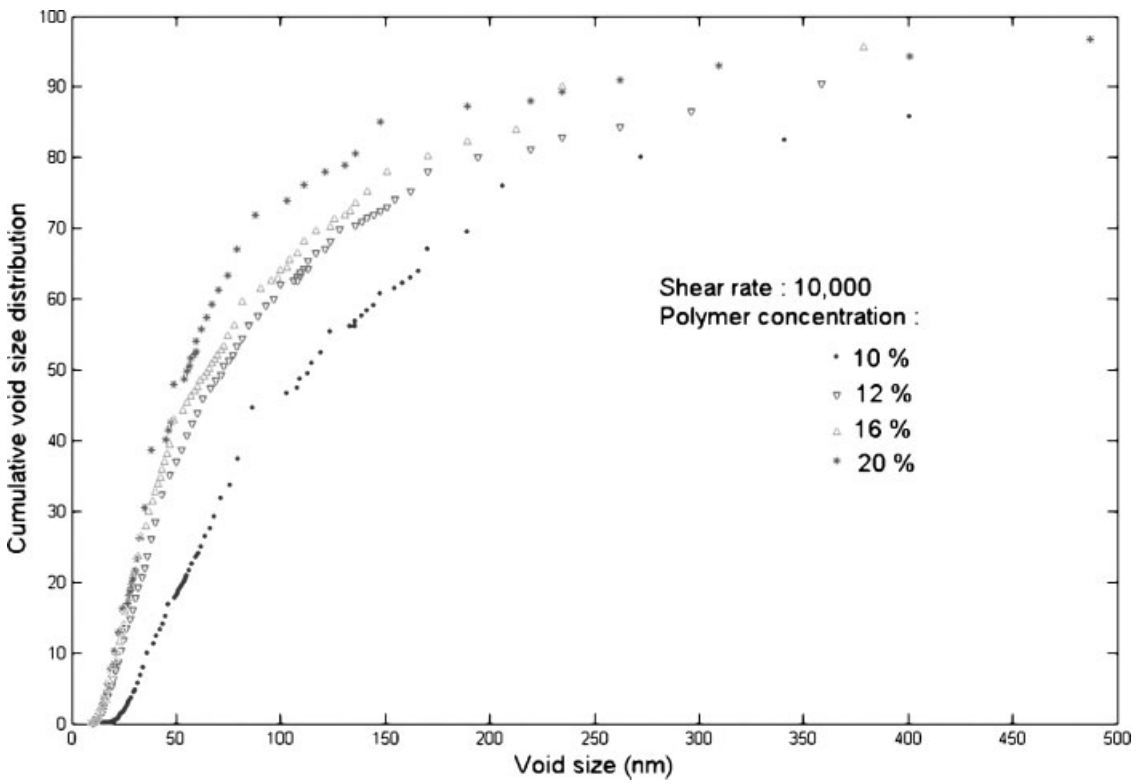

Figure 5 Effect of dope polymer concentration on cumulative nanometer voids distribution of as-spun fibers.

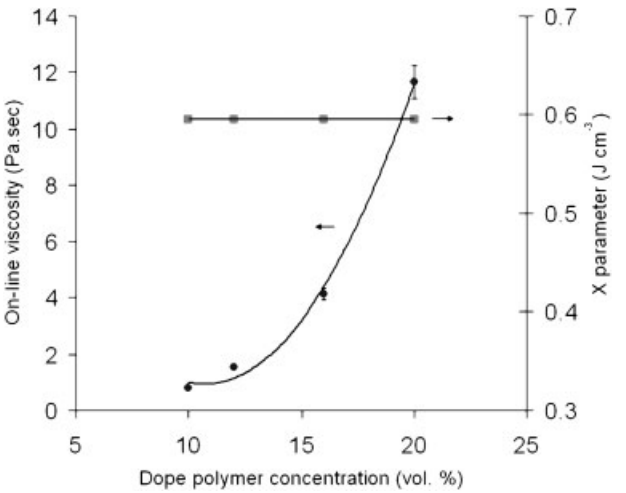

Figure 6 Effect of dope polymer concentration (series A) on fiber precursor on-line viscosity (filled circles) and thermodynamic affinity, X, toward coagulation medium (filled squares).

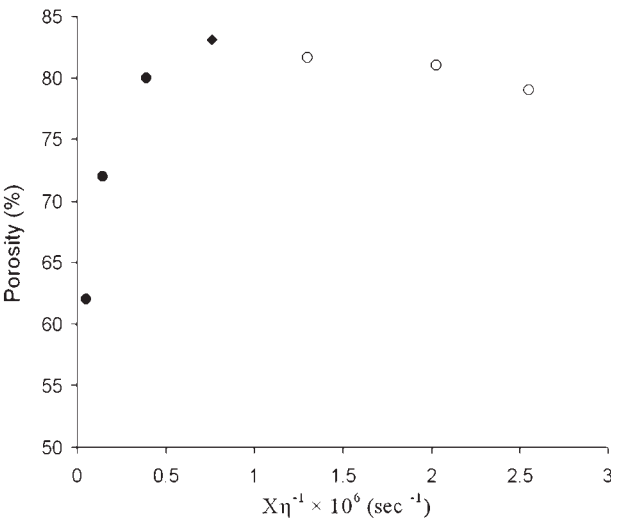

Figure 8 Fiber overall porosity versus X for as spun fibers: series A (filled circles) and series B (empty circles).

polymer affinity toward mixed solvents or nonsolvents can be conducted using the Mayes' model.[30]

By fiber precursor/nonsolvent contact, dope often partitions to polymer lean and rich phases leading to viscosity increment in engulfing polymer reach phase which resist against polymer lean phase (nuclei) growth. Nonetheless, the shells around different nuclei form a matrix containing nanometer and micrometer polymer lean phase particles. Accordingly, dope on-line viscosity measurement can be considered as real resistive situation involved in phase evolution. Overall fiber porosity versus $X\eta^{-1}$ index for all as spun fibers is plotted in Figure 8. While, dope nonsolvent enhancement in 10 vol % polymer solution showed a mild porosity decrement (open circles), dope polymer concentration increment led to notable overall porosity decrement (filled circles). It worth's mentioning that, dope nonsolvent increment in 10 vol % polymer solution and dope polymer concentration enhancement affected overall porosity through $X\eta^{-1}$ index increment and decrement, respectively. Nonsolvent increment in 10 vol % polymer solution changed fiber structure by substituting micrometer voids with nanometer ones

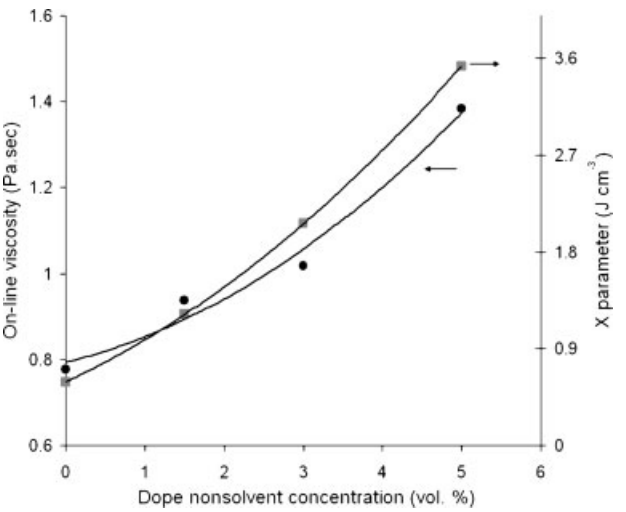

Figure 7 Effect of nonsolvent concentration in 10 vol % polymer solution (series B) on fiber on-line viscosity (filled circles) and thermodynamic affinity, X, toward coagulation medium (filled squares).

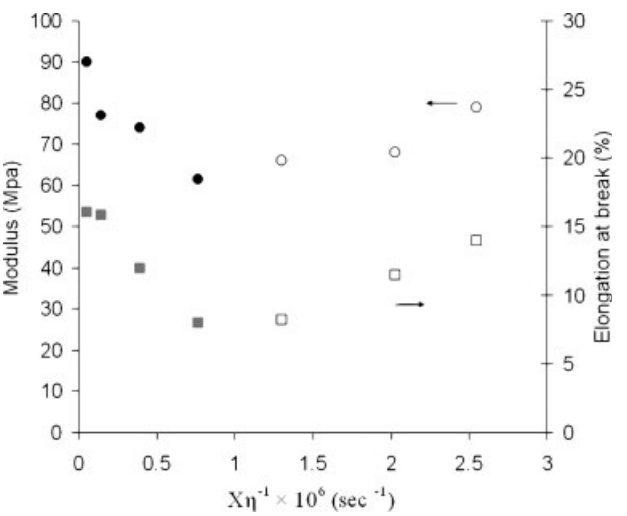

Figure 9 As-spun fibers modulus and elongation at break versus Xh_{21}: series A (filled circles) and series B (open circles).

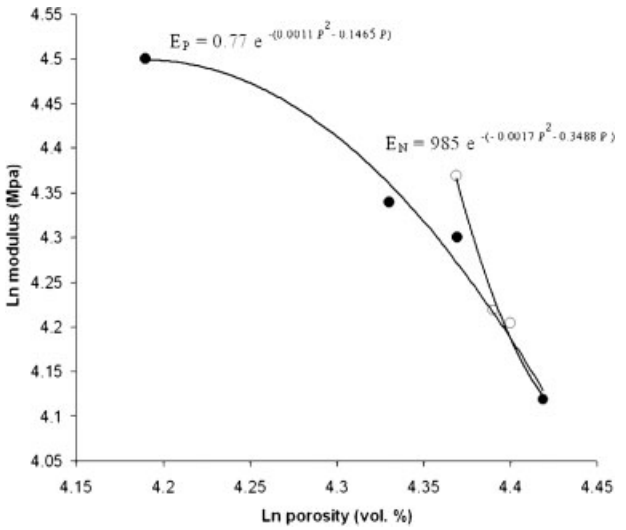

Figure 10 Double logarithmic plot of as-spun fibers modulus versus their overall porosity: series A (filled circles) (E_P) and series B (open circles) (E_N).

through $X\eta^{-1}$ increment and led to mild fiber modulus and elongation at break improvement due to void size reduction, Figure 9. On the other hand, stronger modulus and elongation at break improvements were observed for dope polymer concentration enhancement via $X\eta^{-1}$ decrement, Figure 9. Dope polymer concentration increment reduced as-spun fibers micrometer voids, kept their nanometer voids almost unchanged while increased their dense ligament volume fraction, Table II. Accordingly, higher modulus and elongation at break are observed for these sets of samples due to the fiber cohesive energy density increment. Double logarithmic modulus-porosity correlations of as spun fibers are plotted in Figure 10. Dope nonsolvent increment in 10 vol % polymer solutions increased modulus in a convex function form porosity decrement through void size reduction. On the other hand, dope polymer concentration enhancement increased as-spun fibers modulus through a concave function of porosity decrement due to dense ligament structure formation in expense of micrometer void reduction, Table II. Void amount or size reduction provides cohesive energy density enhancement against chain deformation under stress. In other words, large interfacial tension between the polymer and air filled voids (nonsolvent) multiplied by their interfacial area is the free energy motive for easy chain sliding and concomitant decreased modulus.[31] In other words, affinity to the large interfacial free energy reduction between polymer and its occluded voids can be envisioned as catalyst to decrease energy barriers against molecular flow facilitating fiber elongation.[32]

Experimental modulus-porosity correlations, Figure 10, were also curve fitted to the Eshpriegs [eq. (6)] and Wang's [eq. (7)] models,[26] to assess as-spun fibers morphological evolution mechanisms:

$$E = E_0 e^{-ap} \tag{6}$$

$$E = E_0 e^{-(ap+bp^2)} \tag{7}$$

Where E_0 and p are modulus of the virgin sample and its porosity, respectively, while a and b are Eshpriegs' and Wang's equation constants. A better fitting (Regression of 95.5% in comparison to 85%) was observed for applying the Wang's model on acquired data. Therefore, the phase separation in the practiced wet spinning process may be nominated as a complex solid-liquid phase separation through nonsolvent intrusion and polymer reach phase resistance (concentrated solution, gel) against polymer lean phase growth (dilute solution).

CONCLUSIONS

Dope polymer concentration or nonsolvent concentration in 10 vol % polymer solution increment was used to change wet spun polyacrylonitrile (PAN) fibers void structure and tensile properties. A new defined index $X\eta^{-1}$ could control aforementioned fiber characteristics based on thermodynamic affinity, X, and on-line viscosity, η, of fiber precursor against mass exchange with coagulation medium. The $X\eta^{-1}$ reduction in case of dope polymer concentration increment through some micrometer void substitution with dense polymer ligament led to notable modulus and elongation at break improvement. On the other hand, mild modulus and elongation at break increment was observed through dope nonsolvent increment in 10 vol % polymer solution due to micrometer voids substitution with nanometer ones.

References

1. Yang, S.; Liu, Z. J Membrane Sci 2003, 222, 87.
2. Tsai, J. S.; Lin, H. C. J Appl Polym Sci 1991, 42, 3045.
3. Bahrami, S. H.; Bajaj, P.; Sen, K. J Appl Polym Sci 2003, 89, 1825.
4. Sawai, D.; Kanamoto, T.; Yamazaki, H.; Hisatani, K. Macromolecules 2004, 37, 2839.
5. Jenny, R. Tinctoria 1990, 87, 75.
6. Rohner, R. M.; Zollinger, H. Text Res J 1986, 56, 1.
7. Um, I. C.; Ki, C. S.; Kweon, H. Y.; Lee, K. G.; Ihm, D. W.; Park, Y. H. Int J Biol Macromol 2004, 34, 107.
8. Qin, J. J.; Gu, J.; Chung, T. S. J Membr Sci 2001, 182, 57.
9. Um, I. C.; Ki, C. S.; Kweon, H. Y.; Lee, K. G.; Ihm, D. W.; Park, Y. H. Int J Biol Macromol 2004, 34, 89.
10. Masson, J. C. Acrylic Fiber Technology and Application; Marcel Decker: New York. 1995.
11. Lin, K. Y.; Wang D. M.; Lai, J. Macromolecules 2002, 35, 6697.
12. Lai, J. Y.; Lin, F. C.; Wu, T. T.; Wang, D. M. J Membr Sci 1999, 155, 31.
13. Oh, S. C.; Wang, Y. S.; Yeo, Y. K. Ind Eng Chem Res 1996, 35, 4796.

14. Li, D.; Chung, T. S.; Ren, J.; Wang, R. Ind Eng Chem Res 2004, 43, 1553.
15. Liu, C. K.; Cuculo, J. A.; Smith, B. J Polym Sci Phys Ed 1990, 28, 449.
16. Knaul, J. Z.; Creber, K. J Appl Polym Sci 1997, 66, 117.
17. McKelvey, S. A.; Koros, W. J. J Membr Sci 1996, 112, 29.
18. Smolders, C. A.; Reuvers, A. J.; Boom, R. M; Wienk, I. M. J Membr Sci 1992, 73, 259.
19. Yilmaz, L.; McHugh, A. J. J Appl Polym Sci 1986, 31, 997.
20. Tsay, C. S.; Mchugh A. J. J Polym Sci Phys Ed 1990, 28, 1327.
21. Ruaan, R. C.; Chang T.; Wang, D. M. J Polym Sci Phys Ed 1999, 37, 1495.
22. van de Witte, P.; Dijkstra, P. J.; van den Berg, J. W. A.; Feijen, J. J Membr Sci 1996, 117, 1.
23. Stoyanov, A. I. J Appl Polym Sci 1982, 27, 235.
24. Beder, N. M.; Kabanova, D. M.; Dvoeglazova, I. N.; Perepelitsa, V. A. Fiber Chem 1986, 18, 441.
25. Dutreiz, C.; Satoh, K.; Kamigaito, M.; Yokoyama, H.; Macromolecules 2007, 40, 7433.
26. Sonnenschein, M. F. J Polym Sci Phys Ed 2003, 41, 1168.
27. Hay, J. N.; Laity, P. R. Polymer 2000, 41, 6171.
28. Koningsveld, R.; Kleintjens, L. A. Macromolecules 1971, 4, 637.
29. Petri, H. M.; Wolf, B. A. Macromolecules 1994, 27, 2714.
30. Gonzalez-Leon, J. A.; Mayes, A. M. Macromolecules 2003, 36, 2508.
31. Sawai, D.; Fuji, Y.; Kanamoto, T. Polymer 2006, 47, 4445.
32. Ferry, J. D. Viscoelastic Properties of Polymers; Wiley: New York, 1980.